Ionospheric Response to the Magnetic Storm of 22 June 2015

Gustavo A. Mansilla

Pure and Applied Geophysics
pageoph

ISSN 0033-4553
Volume 175
Number 3

Pure Appl. Geophys. (2018)
175:1139-1153
DOI 10.1007/s00024-017-1741-5

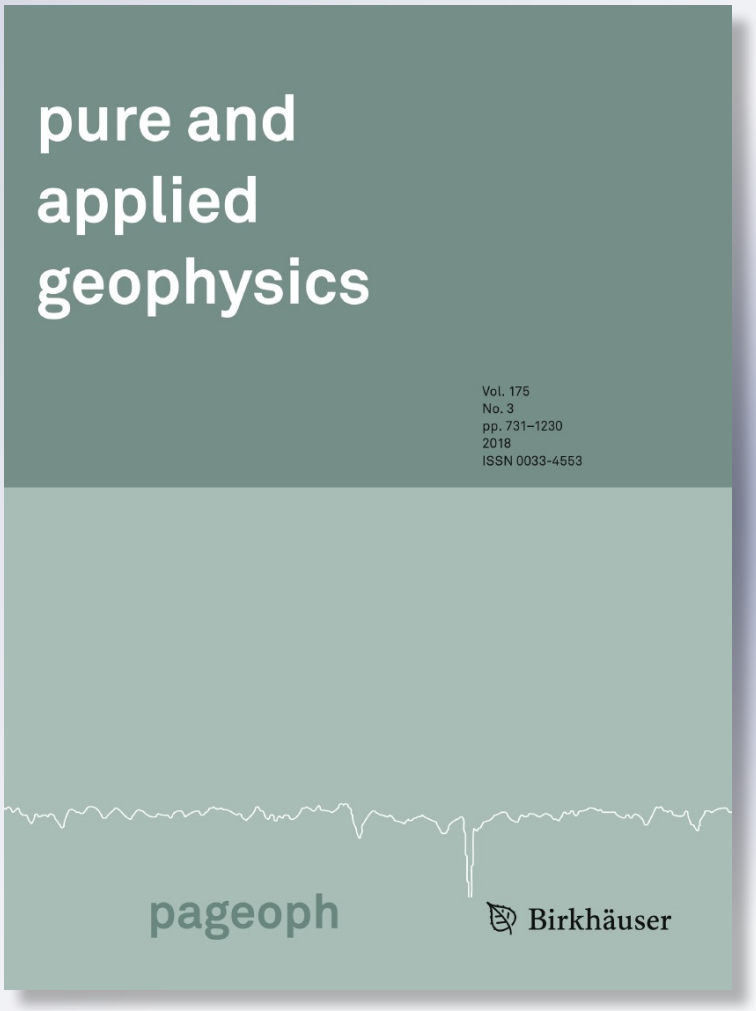

Springer

Pure Appl. Geophys. 175 (2018), 1139–1153

https://doi.org/10.1007/s00024-017-1741-5

Pure and Applied Geophysics

Ionospheric Response to the Magnetic Storm of 22 June 2015

Gustavo A. Mansilla[1,2]

Abstract—A global study is made of the response of the total electron content of the ionosphere (TEC) to the geomagnetic storm occurred on 22 June 2015 (one of the strongest geomagnetic storms of the current Solar Cycle 24). Using data from 44 sites, a hemispheric comparison is made by considering high latitudes (> 50°), middle latitudes (30°–50°) and low latitudes (30°N–30°S). The main features observed were: increases in TEC at high latitudes prior to the storm main phase, a considerable asymmetry of TEC response at middle and low latitudes of the Northern Hemisphere and the Southern Hemisphere and decreases at equatorial latitudes. The long duration enhancements in TEC were well correlated with increases in the O/N_2 ratio but decreases in TEC had not associated decreases in the O/N_2 ratio as occur with the decreases in the electron density. Besides, prompt penetration electric fields can play an important role in the equatorial and low-latitude ionosphere during main phase of the storm.

Key words: Geomagnetic storm, global TEC, physical mechanisms.

1. Introduction

Perturbations of the ionosphere in association with geomagnetic storms are object of a close attention of the specialists on the ionosphere since several decades. Ionospheric storms represent an extreme form of space weather, which has significant, adverse effects on increasingly sophisticated ground and space-based technological systems of our society (Bounsanto 1999).

Many papers have been written about the ionospheric storms. The study of the ionospheric disturbances during geomagnetic storms is generally carried out using either the critical frequency of the F2 layer foF2, or Total Electron Content (TEC) because disturbances of TEC, electron peak density and peak height are produced. Similarly to the peak electron density, during storm periods TEC may either increase or decrease with respect to quiet condition values. Different dynamical and chemical processes, such as energetic particle precipitation, changes of electric field and current systems, traveling atmospheric disturbances, thermospheric circulation, composition changes, etc. have been used to explain the ionospheric features of the electron density during the different phases of the geomagnetic storms at different latitudes. These factors make ionospheric storms complicated.

Although the ionospheric perturbations are studied since several decades ago, neither the morphology nor the physics of the changes is completely known because the complexity and diversity of the physical processes involved. Astafyeva et al. (2015 and references therein) recently mentioned that ionospheric storms are not yet completely understood and remain one of the primary subjects of ionospheric science. Some features of the ionospheric storms still not clear are the strong longitudinal and latitudinal asymmetries, the alternation of positive and negative phases, or the completely different storm-induced disturbance behavior of the ionospheric F2 region above two comparable locations, which are frequently observed (e.g., Habarulema et al. 2013). For that reasons still it is necessary to carry out further studies to clarify several physical mechanisms. Some review articles on ionospheric storms were presented by Rishbeth (1991), Prölss (1995), Abdu (1997), Mendillo (2006), Danilov and Lastovicka (2001), and Danilov (2001, 2013).

Analyzing a set of storms for a particular location can carry out a study of the F-region storm effects.

[1] Departamento de Física, Facultad de Ciencias Exactas y Tecnología, Universidad Nacional de Tucumán., Av. Independencia 1800, 4000 San Miguel de Tucumán, Argentina. E-mail: gmansilla@herrera.unt.edu.ar

[2] Consejo Nacional de Investigaciones Científicas y Técnicas, Godoy Cruz 2290, Buenos Aires, Argentina.

Another approach is to examine an individual event for a large network of stations globally distributed (the so-called case studies). Case studies, which consider several stations of different latitudinal regions, are important for a view of space weather and for the understanding of the role of various physical mechanisms during ionospheric storms. In this paper we analyze the global disturbances of the Total Electron Content (TEC) occurred in response to the storm occurred on 22 June 2015 (with sudden commencement at $\sim$ 18 UT) and discuss the main physical mechanisms involved in such disturbances. This was one of the strongest geomagnetic storms of the current 24 solar cycle (the "Solstice" storm). The storm onset information was obtained of the Monthly Bulletin of the International Service of Geomagnetic Indices (http://isgi.unistra.fr).

The ionospheric response to this intense geomagnetic storm has been studied in some confined sectors. Singh and Sripathi (2017) analyzed the response of equatorial and low latitude ionosphere with GPS receivers over the Indian stations Tirunelveli (8.73°N,77.70°E; geom: 0.32°N), Hyderabad (17.36°N, 78.47°E; geom: 8.76°N), and Allahabad (25.45°N, 81.85°E; geom: 16.5°N). They observed oscillatory behavior in the foF2, h'F (km) and TEC during both main and recovery phases. On 24 June, a decrease of electron density was observed at Allahabad/Hyderabad and an increase of density over Tirunelveli. Using data from the three Swarm satellites, Astafyeva et al. (2016) observed during the development of the main phase of the storm a significant dayside increase of the vertical total electron content (VTEC) and electron density at low latitudes on the dayside. From $\sim$ 22 UT of 22 June to $\sim$ 1 UT of 23 June, the dayside experienced a strong negative ionospheric storm, while on the nightside an extreme enhancement of the topside VTEC occurred at mid-latitudes of the northern hemisphere.

This geomagnetic storm occurred after a long-duration quiet geomagnetic period, which permits us to assume that ionospheric disturbances are really caused by the storm with no overlapping of other effect. The interval 21–24 June 2015 was selected for this study. The Dst index reached a minimum value of $-$ 204 nT during the storm. According to Gonzales et al. (1994), geomagnetic storms with Dst $\leq -$ 100 nT are classified as intense storms.

Section 2 contains description of data used in the analysis, Sect. 3 deals with the disturbances in TEC and Sect. 4 presents a discussion of the possible driver mechanisms for the effects observed. The paper is closed with brief conclusions.

2. Data

We employed the Total Electron Content data from 44 stations, which are listed in Table 1, for the period 21–24 June 2015. Their locations are plotted in Fig. 1. Data for these stations are available in the web site of the Izmiran Pushkov Institute of Terrestrial Magnetism, Ionosphere and Radio Waves Propagation of the Russian Academy of Sciences (http://www.izmiran.ru/services/iweather/tec/), which provides products of the International GPS Service for Geodynamics (IGS) in the form of Receiver Independent Exchange Format (RINEX) files. The source of these data is JPL (Jet Propulsion Laboratory, Pasadena, California, USA).

The different phases of the magnetic storm were determined by the variation in Dst geomagnetic index. Hourly values of Dst and AE indices were taken from the World Data Center (WDC) Kyoto, Japan website http://wdc.kugi.kyoto-u.ac.jp/dstae/index.html.

To observe the heliospheric structure, which has caused this storm, we used the Bz component of the Interplanetary Magnetic Field (IMF) and the speed and proton density of the solar wind measured aboard the Advanced Composition Explorer satellite (http://www.swpc.noaa.gov/products/ace-real-time-solar-wind).

Data of the interplanetary electric field provided by OMNIweb data (NASA, Goddard Space Flight Center, http://omniweb.gsfc.nasa.gov) were also used. This electric field was computed as $\mathbf{E} = -\mathbf{V} \times \mathbf{Bz}$, where **Bz** is the southward component of the IMF and **V** the bulk speed.

For the analysis, we use five sectors based on the geomagnetic latitude, as used by Kane (2005):

Table 1

Stations used in this study

	Geog. Lat.	Geog. Lon. (E)	Geomag. Lat.	Geomag. Long. (E)
Sector I				
Murmank	69.0	33.0	64.1	126.8
Sodankyla	67.4	26.6	63.7	120.3
Dikson	73.5	80.4	63.0	161.7
Lovozero	67.9	35.0	62.9	127.4
Amderma	69.5	61.4	61.0	147.7
Salekhard	66.7	66.7	57.3	149.8
Gorkovskaya	60.3	29.4	56.3	106.1
Kaliningrad	54.7	20.6	53.1	105.8
Dourbes	50.1	4.6	51.9	88.1
Chilton	51.5	358.7	51.8	78.8
Yakutsk	62.0	129.7	51.0	194.1
Moscow	55.5	37.3	50.8	120.9
Magadan	60.1	151.0	50.7	210.8
Novosibirsk	55.0	82.9	44.1	157.8
Sector II				
Pruhonice	50.0	14.5	49.9	97.3
Wallops Is	37.8	284.5	49.2	353.9
Boulder	40.1	254.8	48.9	318.7
Tomsk	56.5	84.9	45.9	159.9
Tortosa	40.4	0.3	43.8	79.9
Rome	41.8	12.5	42.5	93.2
Rostov	47.2	39.7	42.4	119.6
Manzhouli	49.6	117.5	38.4	186.5
Wakkanai	45.4	141.7	35.5	207.3
Sector III				
Ramey	18.5	292.8	30.0	2.5
Beijing	40.0	116.3	28.8	174.1
Kokubunji	35.7	139.5	25.5	205.8
Yamagawa	31.2	130.6	20.6	199.1
Chongqing	29.5	106.4	18.2	177.1
Okinawa	26.3	127.8	15.5	196.9
Hainan	18.3	109.3	7.8	180.2
Jicamarca	12.0 S	283.2	0.6 S	353.7
Darwin	12.4 S	130.9	22.9 S	202.7
Cocos Is	12.2 S	96.8	23.2 S	165.4
Townsville	19.3 S	146.7	28.5 S	220.4
Sector IV				
Perth	31.9 S	115.9	44.5 S	186.5
Canberra	35.3 S	149.0	44.0 S	224.8
Grahamstown	33.3 S	26.5	33.7 S	88.4
Hermanus	34.4 S	19.2	33.4 S	81.0
Port Stanley	51.7 S	302.2	40.6 S	10.3
Brisbane	27.5 S	152.9	35.4 S	228.3
Norfolk	29.0 S	168.0	34.5 S	244.6
Sector V				
Scott Base	77.9 S	166.8	78.9 S	294.8
Mawson	67.6 S	62.9	73.3 S	103.5
Hobart	42.9 S	147.2	51.4 S	225.9

Sector I: Northern Hemisphere (NH) high latitudes ($> 50°$N)
Sector II: Northern Hemisphere (NH) middle latitudes (30°N–50°N)
Sector III: NH and SH (30°N–30°S)
Sector IV: Southern Hemisphere (SH) middle latitudes (30°S–50°S)
Sector V: Southern Hemisphere (SH) high latitudes ($> 50°$ S)

The disturbance degree of TEC during the storm was estimated by the deviation from an average of quiet days of the moth of the storm:

$$\mathrm{DTEC} = (\mathrm{TECobs} - \mathrm{TECavg}) \times 100/\mathrm{TECavg}\%$$

where TECobs is the observed value of the total electron content during storm period and TECavg is the average value of the five quiet days: June 2 (Q3), June 3 (Q5), June 4 (Q4), June 5 (Q2) and June 6 (Q7). Here we called positive (negative) disturbance to positive (negative) values of DTEC.

3. Results of Observations

Figure 2 illustrates the variation of the geomagnetic indices Dst and AE, the component Bz of the interplanetary magnetic field (IMF), the solar wind speed and the proton density during the period 21–24 June 2015. The sunspot AR2371 erupted on June 21 at 01:42 UT, producing an M2-class solar flare and a full-halo CME. The magnetic storm started at about 18 UT on 22 June.

The different phases of the storm defined by the Dst behavior, namely initial phase, main phase and recovery phase are shown in the top plot of Fig. 2. The initial phase and the main phase were from the storm sudden commencement SSC (18 UT on 22 June) to about 19 UT on June 22 and from 19 UT to Dst (min) = − 204 nT at 05 UT on 23 June (End of the Main Phase-EMP), respectively. A long recovery phase occurred after EMP (during most of 23 June and also on 24 June). The initial phase is caused by the interaction of a solar wind disturbance with the

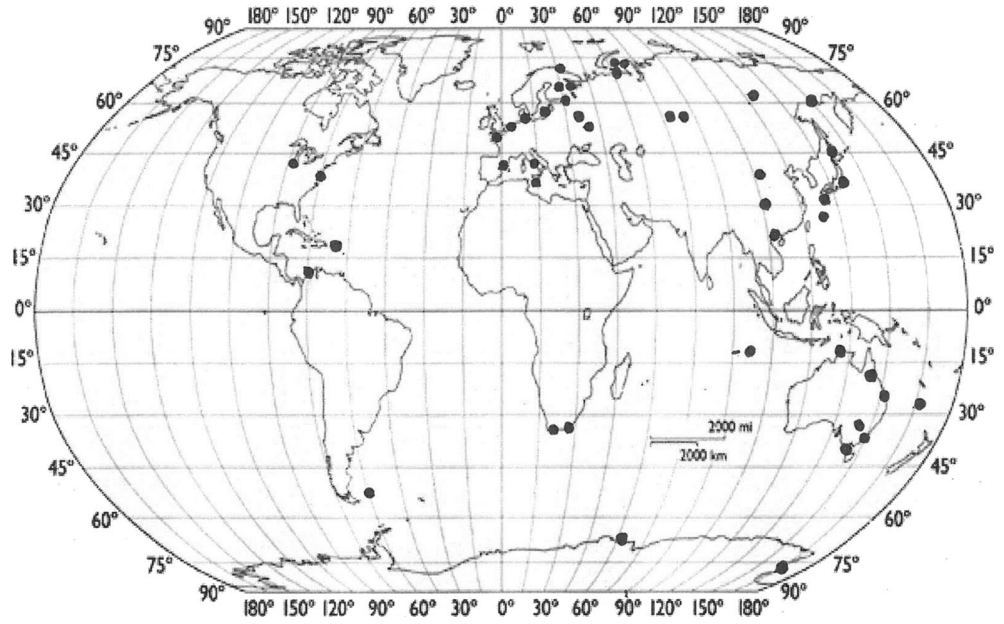

Figure 1
Map of the stations used in the analysis, in geographic coordinates

geomagnetic field; the main phase of the storm is due to the growth of the ring current in the magnetosphere while the recovery phase is consequence of the ring current decay by collisional processes. Vertical lines indicate the starting and the end of the main phase (or onset of the recovery).

The AE index (which is a measure of currents in the auroral electrojet) started to increase at about 06 UT on 22 June and reached a secondary peak of 850 nT at 08 UT, it decreased abruptly at 12 UT and increase again reaching a peak of about 1600 nT simultaneously with the storm onset. It decreased near to the end of the main phase and increased again during the recovery phase, showing fluctuations, indicative of energy injection (substorm activity) at auroral latitudes due to Joule heating. The interplanetary magnetic field (IMF) Bz component showed an oscillating behavior. It sharply turned southward at about 03 UT of June 22 and reached the minimum of – 30 nT at 18 UT but became northward (positive) at about 20 UT, remaining thus during about 6 h. The IMF Bz turned southward again at 00 UT on 23 June and remained largely negative during about 12 h, reaching approximately – 23 nT at 02 UT on June 23. The observed period with negative IMF Bz led to the interconnection between the IMF and the Earth's magnetic field lines and produces the significant Dst decrease (− 204 nT). The solar wind velocity started to increase at about 14 UT on the storm day, showing a sharply increase at about 18 UT on 22 June (the initial phase of the storm). The solar wind velocity jumped from ∼ 440 to ∼ 680 km/s. The proton density also abruptly increased from ∼ 5 to ∼ 30 cm^{-3} at 11 UT on June 21. In general, the proton density remained with enhanced values till about 02 UT on 23 June when an important decrease was produced.

Below we will focus our attention mainly on the period from ∼ 18 UT on 22 June to ∼ 05 UT on 23 June, which includes the initial and the main phases of the storm.

3.1. Sector I: Northern Hemisphere (NH) High Latitudes (> 50°N)

Figure 3 shows the disturbances of TEC for this sector during the storm period 21–24 June 2015. In this sector, the storm commencement occurred at nighttime hours, between before local midnight and predawn hours. Before the storm commencement, no

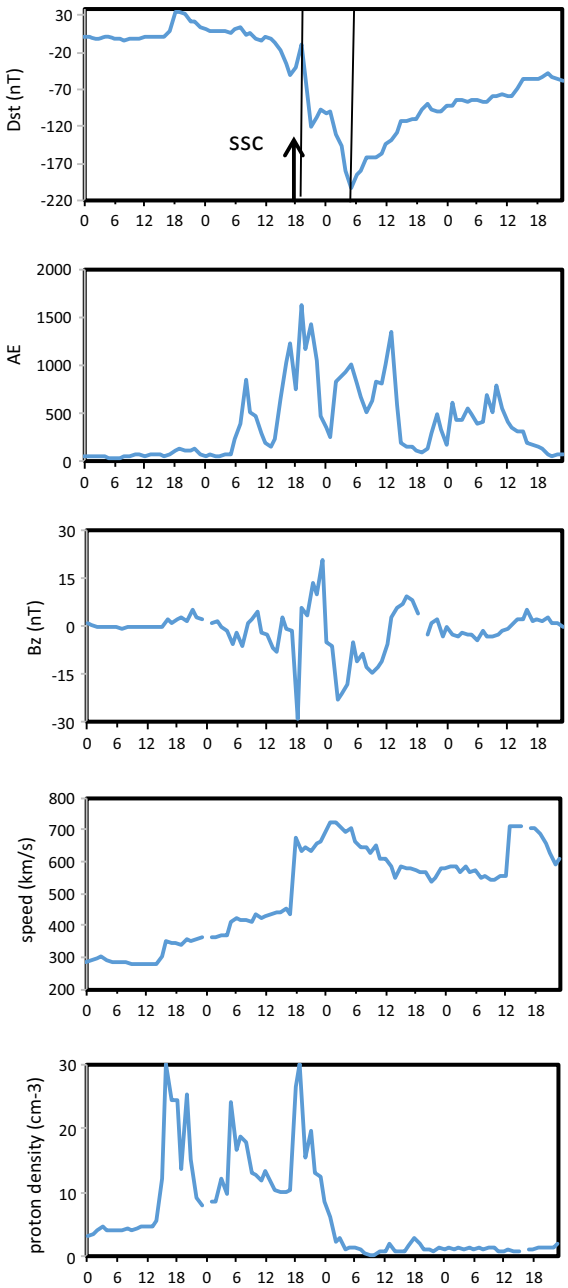

Figure 2
Hourly variations of the Dst and AE geomagnetic indices, the Bz component of the Interplanetary Magnetic Field, the speed and proton density of the solar wind for the period 21–24 June 2015. The arrow indicates the storm sudden commencement

significant positive disturbances were observed. The common feature at the stations irrespective of their location was long decreases in TEC (with respect to quiet time values), in general thereafter the storm onset, which remained throughout storm period. The more eastern stations (Yakutsk, Magadan) presented decreases in TEC prior to the initial phase. In general, the maximum decreases occurred nearly coincident with EMP and reached ∼ 50% excepting at Yakutsk, Magadan and Novosibirsk where the maximum decreases (∼ 60%) were between 12 UT and 18 UT on June 23.

3.2. *Sector II: Northern Hemisphere (NH) Middle Latitudes (30°N–50°N)*

Figure 4 shows the variations of DTEC at the stations of this sector. The storm started in this sector in the afternoon-midnight hours. At Wakkanai the storm commencement occurred during dawn hours. A significant enhancement occurred at Wallops Is between about 20 UT on 22 June and 00 UT on 23 June (between 15 and 20 LT), during the development of the main phase. Tortosa and Gibilmanna also presented increases in TEC from before the storm onset till about 02 UT on 23 June (local midnight on 22 June to after local midnight on 23 June). The positive disturbances in DTEC changed to negatives during the end of the main phase and the recovery phase. The rest of the stations, with no significant disturbances initially, presented negative DTEC values during the main phase and recovery phase. The maximum decreases in TEC occurred in general during the first part of the recovery and reached ∼ 50–60%.

3.3. *Sector III: NH and SH (30°N–30°S)*

Figure 5 presents the variations of DTEC for the stations located in this sector. In general, the main phase of the storm occurred from past local midnight to afternoon hours. At Ramey and Jicamarca, the more eastern stations, the main phase occurred in the afternoon-midnight hours. It can be seen a marked hemispheric asymmetry in response to the storm. The Northern Hemisphere stations and Jicamarca (equatorial) showed small negative disturbances or a short-lived positive disturbance (at Ramey) during the main phase. Between 00 UT and 06 UT on 23 June, negative disturbances started at all the stations of the Northern Hemisphere, which remained during the

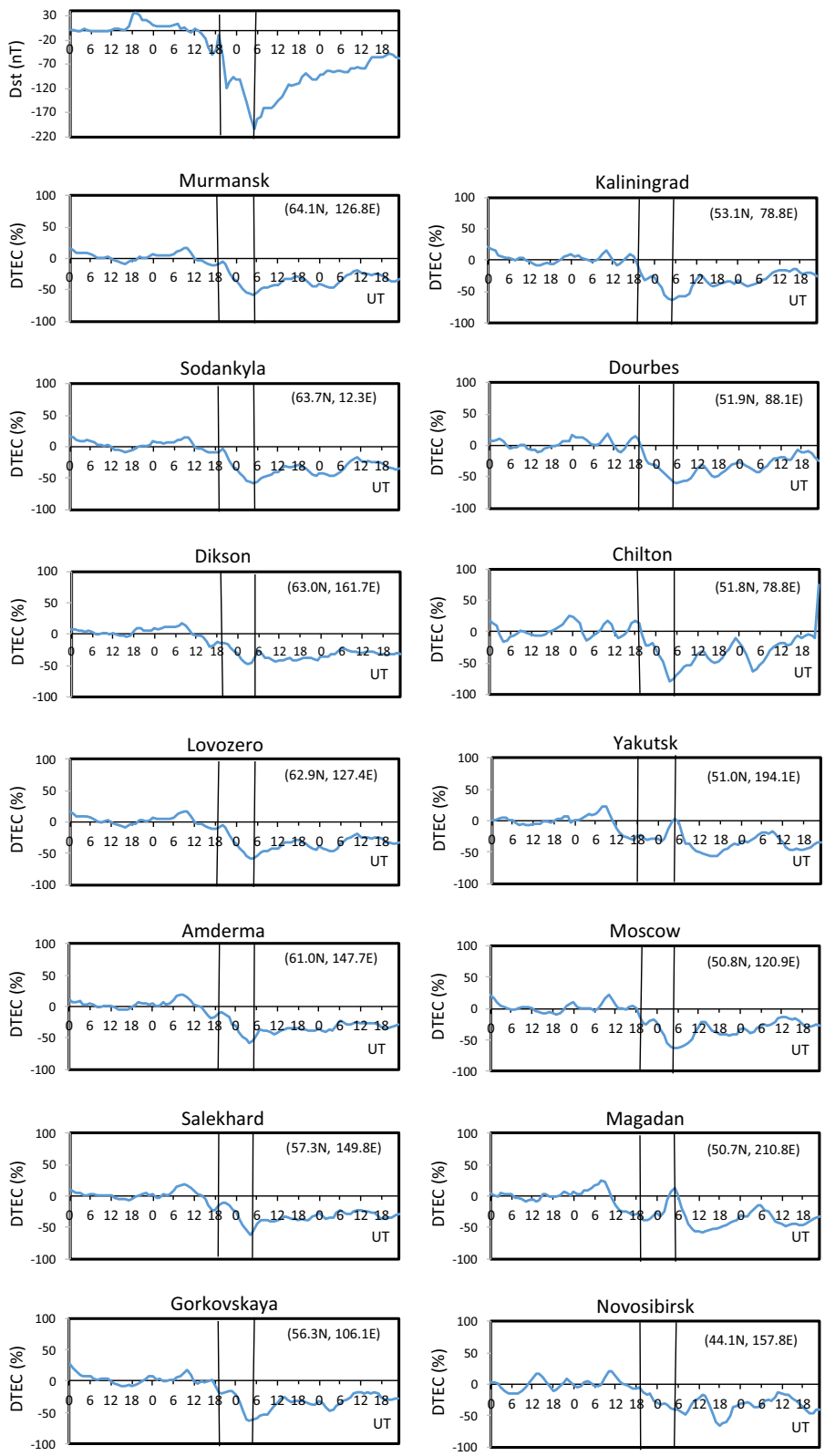

◀Figure 3
Relative deviations with respect to quiet days of the total electron content from the stations located in *sector I* for the period 21–24 June 2015

recovery phase. Jicamarca showed a recovery to quiet time values on 24 June. The southern hemisphere stations presented irregular positive disturbances since about 19–20 UT on June 22 till 16–18 UT on

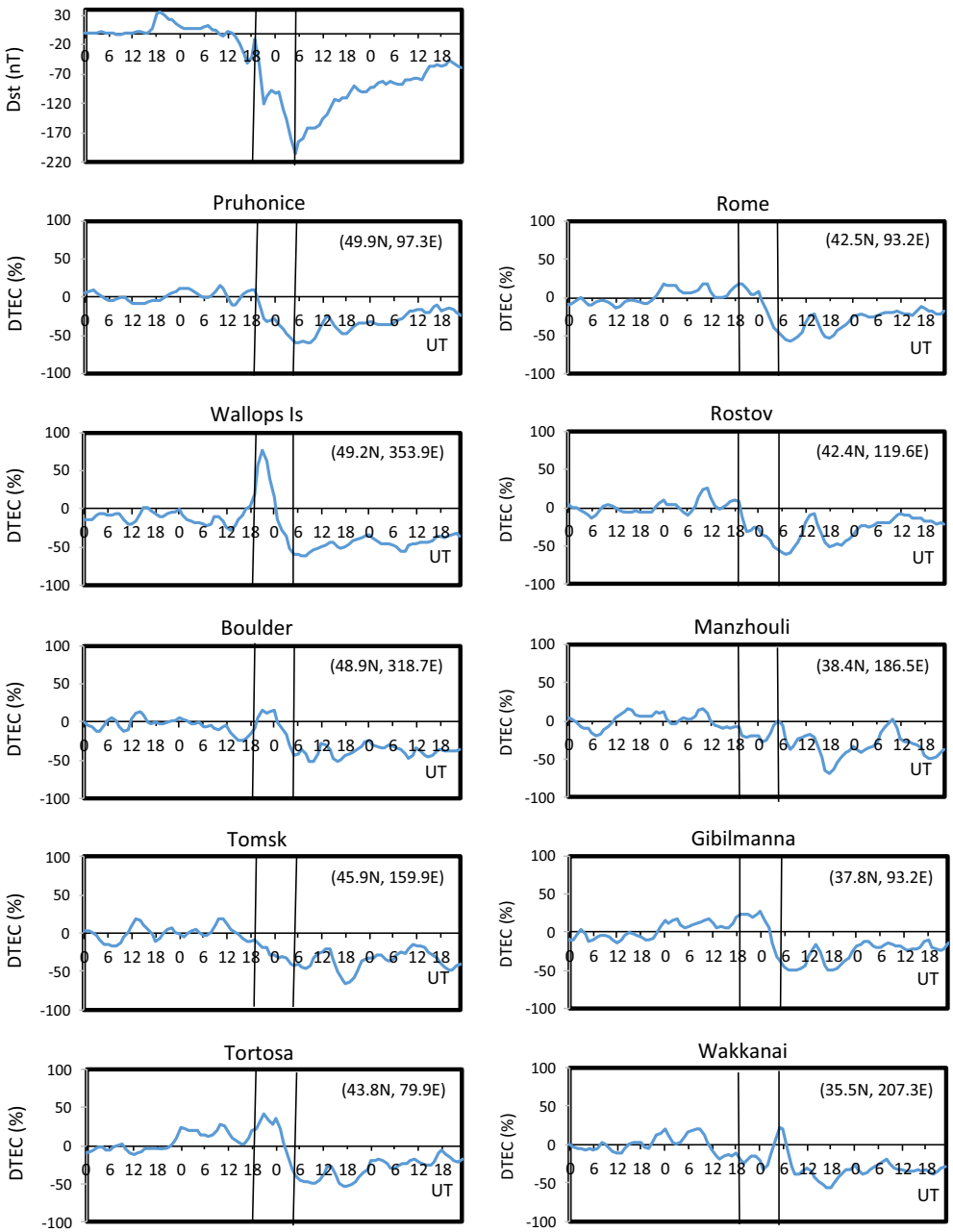

Figure 4
Relative deviations with respect to quiet days of the total electron content from the stations located in *sector II* for the period 21–24 June 2015

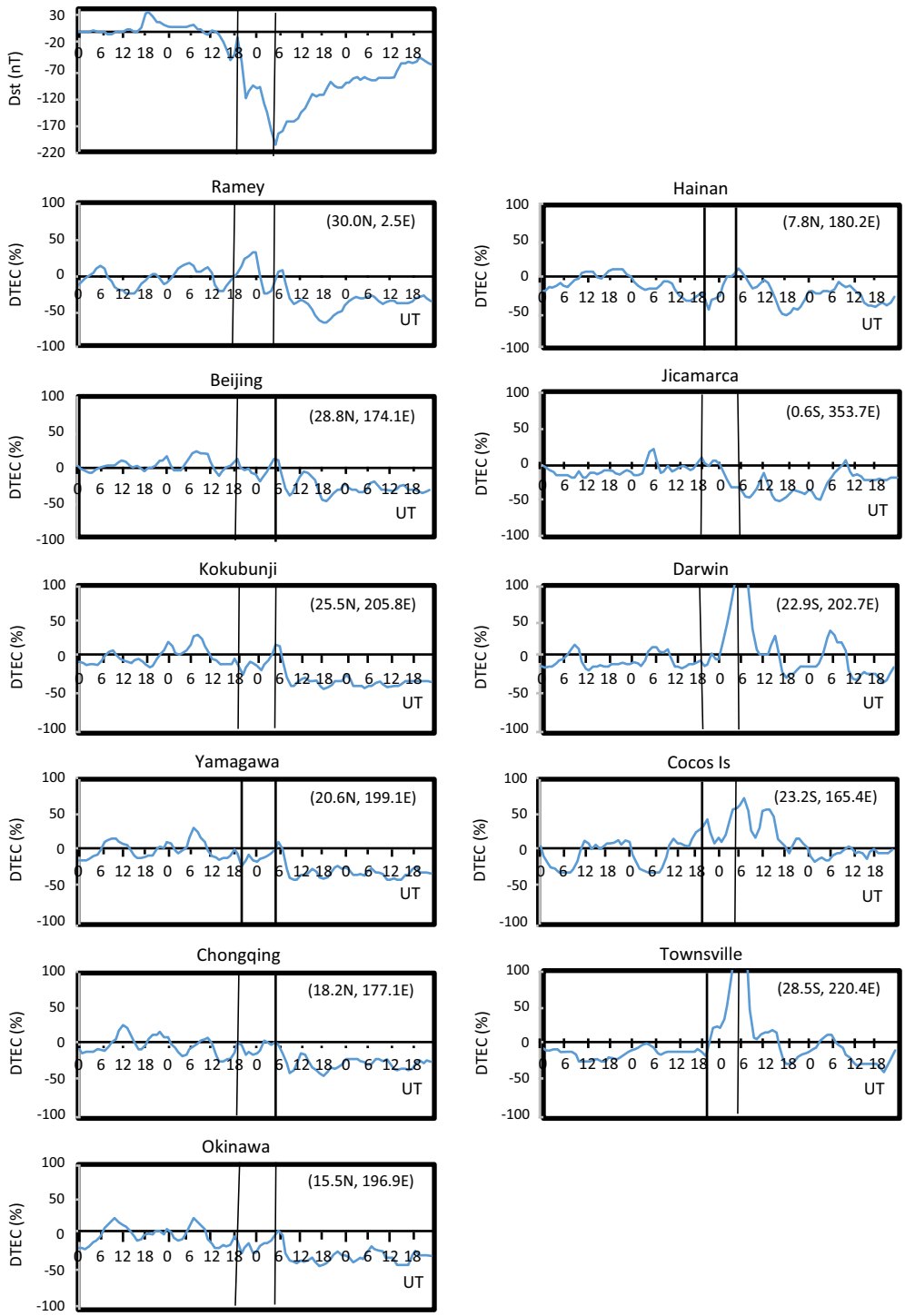

Figure 5
Relative deviations with respect to quiet days of the total electron content from the stations located in *sector III* for the period 21–24 June 2015

23 June. At Darwin and Townsville, the positive values of DTEC exceeded 100% near the minimum Dst (in the afternoon hours). These effects were followed by minor negative disturbances during the recovery.

3.4. *Sector IV: Southern Hemisphere (SH) Middle Latitudes (30°S–50°S)*

Figure 6 shows the hourly DTEC deviations from 21 June to 24 in sector IV. The main phase in general occurred between after dusk and local dawn in this

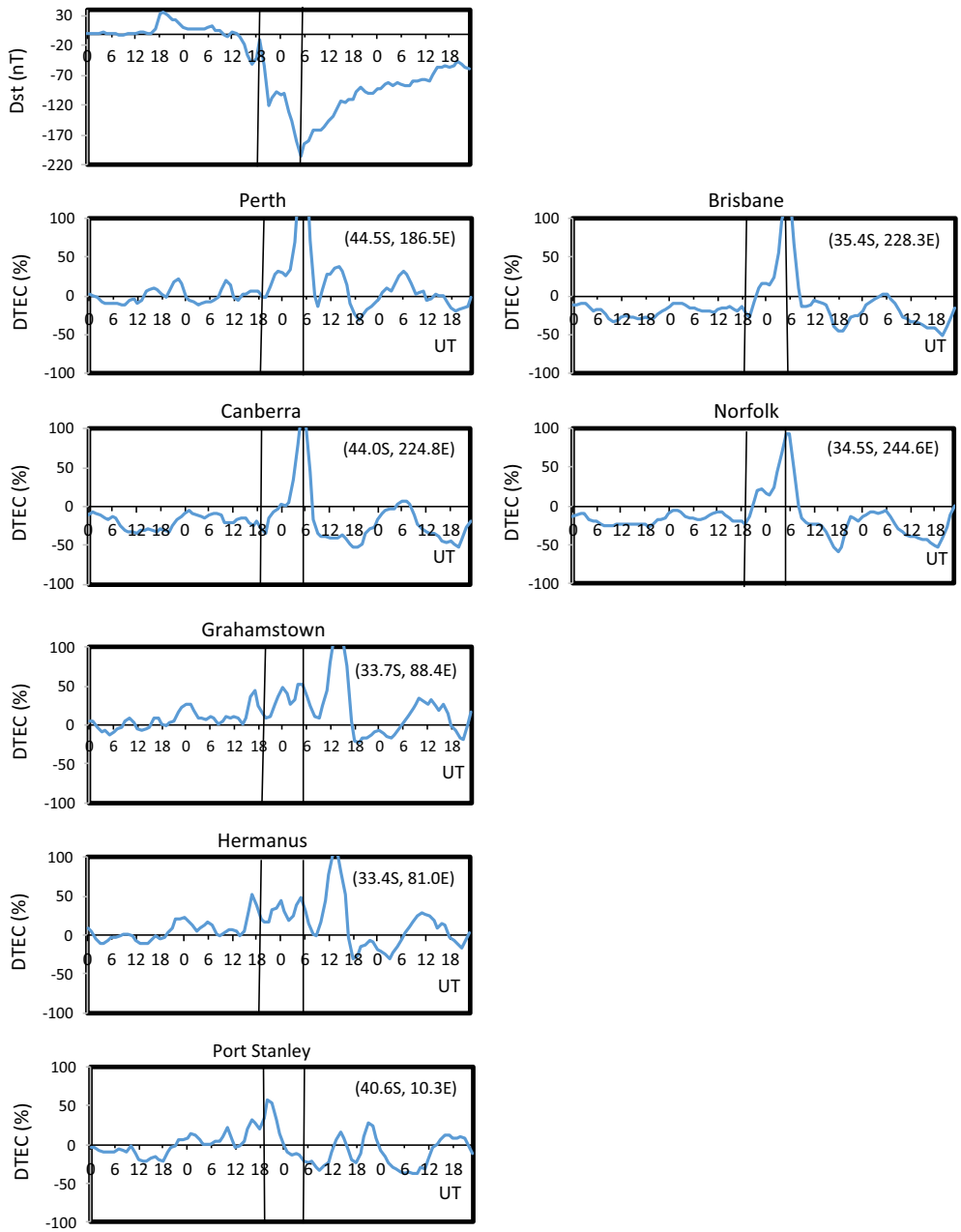

Figure 6
Relative deviations with respect to quiet days of the total electron content from the stations located in *sector VI* for the period 21–24 June 2015

sector. At the Australian stations (Canberra, Brisbane and Norfolk), the main phase occurred from local sunrise to afternoon hours. There is a considerable longitudinal variation in this sector. Short-lived positive disturbances (~ 7–8 h) were observed at the easternmost stations (Canberra, Brisbane and Norfolk) between about 20–22 UT on 22 June and 07–08 UT on 23 June. The peak enhancements (~ 100% change) occurred almost 2 h after the minimum Dst. These positive disturbances were followed by negative disturbances (~ 50% maximum change). Positive disturbances initiated at Grahamstown, Hermanus and Port Stanley about 12–14 UT on 22 June (prior to the initial phase), remained until about 00 UT and 18 UT the next day at Port Stanley—Grahamstown and Hermanus respectively. These disturbances reached ~ 100% at the South African stations during the recovery (in the daytime hours) and were followed by negative disturbances between about 18 UT on 23 June and 06 on 24 June, and the positive disturbance over Port Stanley changed to negative one during about 10–12 h.

3.5. *Sector V: Southern Hemisphere (SH) High Latitudes (> 50°S)*

Figure 7 shows the variation of DTEC for the stations of this sector. The storm commencement occurred in the midnight-predawn hours in this sector. The higher latitude station Scott Base presented a significant increase in TEC from before the storm commencement to the end of the main phase. During the first part of the recovery, the total electron content decreased during about 12 h (~ 50% maximum change) and after that slightly increased. Mawson also presented a positive disturbance prior to the storm onset, which remained throughout the main phase and then was followed by a negative disturbance during 4–6 h (~ 50% maximum change). At Hobart, two minor positive peaks were observed during the main phase of the storm and a negative storm disturbance (~ 18 h of duration) during the recovery phase.

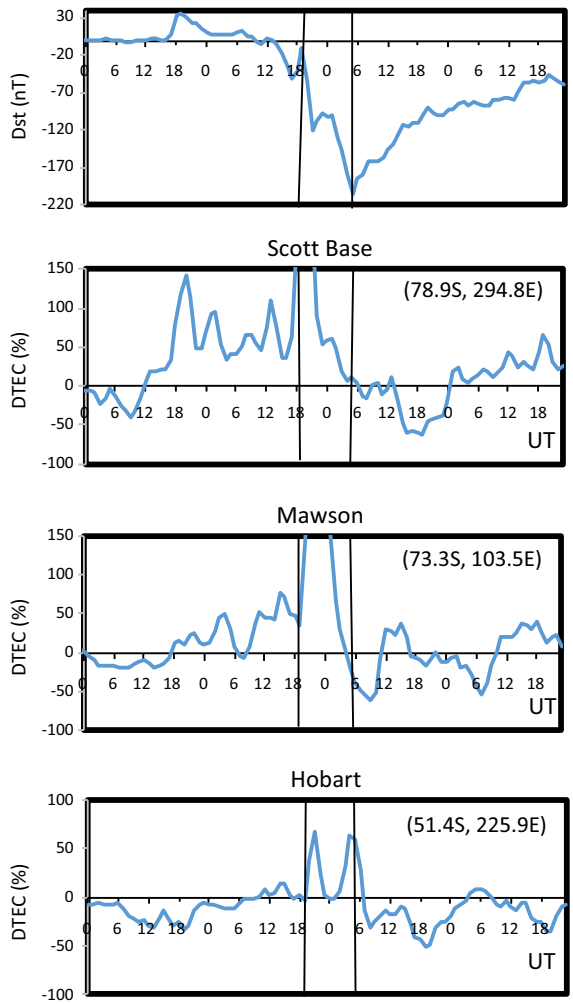

Figure 7
Relative deviations with respect to quiet days of the total electron content from the stations located in *sector V* for the period 21–24 June 2015

3.6. *Summary of the Effects Observed During the Main Phase*

Figure 8 presents a summary of the ionospheric effects observed during the development of the main phase (00 UT–05 UT on 23 June). White circles represent positive disturbances and black circles represent negative disturbances. Under disturbed conditions, it can be seen that in general, the middle latitude stations of the summer hemisphere considered in this study presented a depletion in the total electron content and in the winter hemisphere the opposite effect was seen. In particular, for the North and South American sectors only few stations are

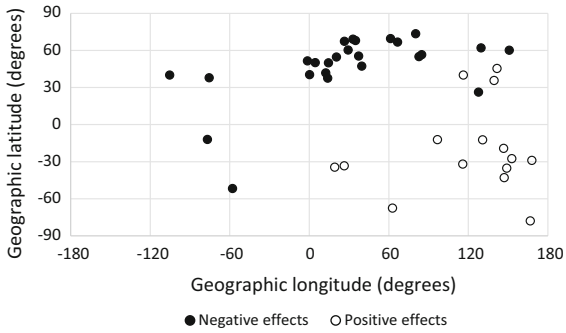

Figure 8
Latitudinal and longitudinal distribution of TEC disturbances between 00 UT and 06 UT on 23 June (during the main phase of the storm). White circles represent positive disturbances and black circles represent negative disturbances

involved in the analysis. Thus, these results may not be entirely representative.

4. Discussion

The global evolution of TEC was examined during the geomagnetic storm occurred on 22 June 2015. For that, we analyzed the relative deviation of hourly TEC values from a diurnal variation curve obtained as an average of five quiet geomagnetic days of the month of the storm. Data from 44 stations was considered.

The following was observed:

There is a considerable asymmetry between northern middle latitudes (summer hemisphere) and southern middle latitudes (winter hemisphere). Remarkable decreases in the total electron content started in general at mid-latitude stations throughout the northern hemisphere during the development of the main phase. This decrease is independent on longitude and occurred over a wide range of local times. Positive disturbances may be also observed at some stations during the main phase, possibly indicative of regional effects. The southern hemisphere stations (winter), presented positive disturbances of different duration during the main phase: relatively short-duration effects ($\sim$ 7–8 h) occurring in general during the daytime hours, and longer-duration effects remaining till the first part of the recovery in the local night-time hours (the South-African stations, Grahamstown and Hermanus). All these positive disturbances changed to negative during the recovery phase of the storm.

At high latitudes is not clear such asymmetry possibly because the Southern Hemisphere stations have higher geomagnetic latitude than the Northern Hemisphere stations.

By comparing DTEC values at Magadan and Hobart (geomagnetic latitudes 50.7°N and 51.4°S and geomagnetic longitudes 210.8°N and 225.9°N, respectively), it can be observed that the NH station presented negative values during the main and recovery phases and the SH station presented positive values during the main phase (in the morning hours), followed by a negative disturbance during the recovery.

In general, the NH higher latitude stations ($> 50°$) presented predominantly negative disturbances without obvious shift in LT and the higher latitude stations of the SH ($> 70°$) presented positive disturbances from before to the storm commencement, whose intensity increased during the main phase.

At NH and SH low latitudes (30°N–30°S) there is substantial difference. The dominant feature at the NH stations was a no significant negative disturbance ($\sim$ 20% maximum change) during the main phase, which increased during the recovery phase. The most striking feature in the SH stations was a significant positive disturbance during the main-recovery phases between the morning and the nighttime hours, followed by a less intense negative disturbance.

4.1. Negative Disturbances

It is well known that changes in the thermospheric composition caused by the heating of the thermosphere during geomagnetic storms are usually used to explain the *negative storm effects* (decreases in the peak electron density) (e.g., Fuller-Rowell et al. 1994; Prölss 1995 and references therein). This is because the thermospheric heating at high latitudes increases the scale height of all neutral species including molecular nitrogen N_2, which in turn leads to a decrease in the ratio O/N_2 at heights of the ionospheric F region. As the atomic oxygen O is the primary source of ionization at F region heights, and the molecular nitrogen is the primary source of recombination, the change of this ratio affects the

daytime electron density. Thus, the daytime decrease of this ratio leads to the negative disturbances in electron density at heights of the ionospheric F region (e.g., Rishbeth and Garriott 1969). However, at night when the main ionization source is absent, the molecular nitrogen plays the dominant role in the electron density control by neutral composition variation.

We used the O/N_2 ratio measured by the Global Ultraviolet Imager (GUVI) on the Thermosphere Ionosphere Mesosphere Energetics and Dynamics (TIMED) satellite to analyze the correlation between negative disturbances in TEC and decreases in the O/N_2 ratio (thermospheric column number density ratio of O and N_2). Figure 9 shows the O/N_2 ratio on 21–24 June (days 23 and 24, part of the main phase and recovery). 21 June is taken as reference (control) day. On 23 June, the O/N_2 ratio was slightly enhanced compared with values on 21 June in the NH in the latitude range 30°–70° and longitude range 0°–100° in association with the negative disturbances observed in this sector. It is interesting to note that over the South-African and Australian sectors, where positive disturbances were observed, the O/N_2 ratio was largely increased compared with values before the storm. On 24 June, the O/N_2 ratio tends to have similar values to those prior to the storm (21 June).

The expected patterns indicate that negative storm effects in the peak electron density frequently occur at mid latitude in summer hemisphere. These negative effects reach lower latitudes in summer than in winter and have a preference for the night and morning sectors due to the local time variation of the neutral winds (Danilov 2001). The TEC behavior in the summer hemisphere during the storm period presents seasonal dependence similar to electron density. However, the observations of the O/N_2 ratio indicate that the responsible physical mechanism for the negative disturbances in TEC seems to be not the same that for the decreases in the peak electron density (negative storm effects) because no decrease in the O/N_2 ratio is observed at the stations with decreased TEC. Instead, there is a clear correlation between positives disturbances and increases in the O/N_2 ratio. Sometimes, such a lack of association between negative disturbances and decreases in the

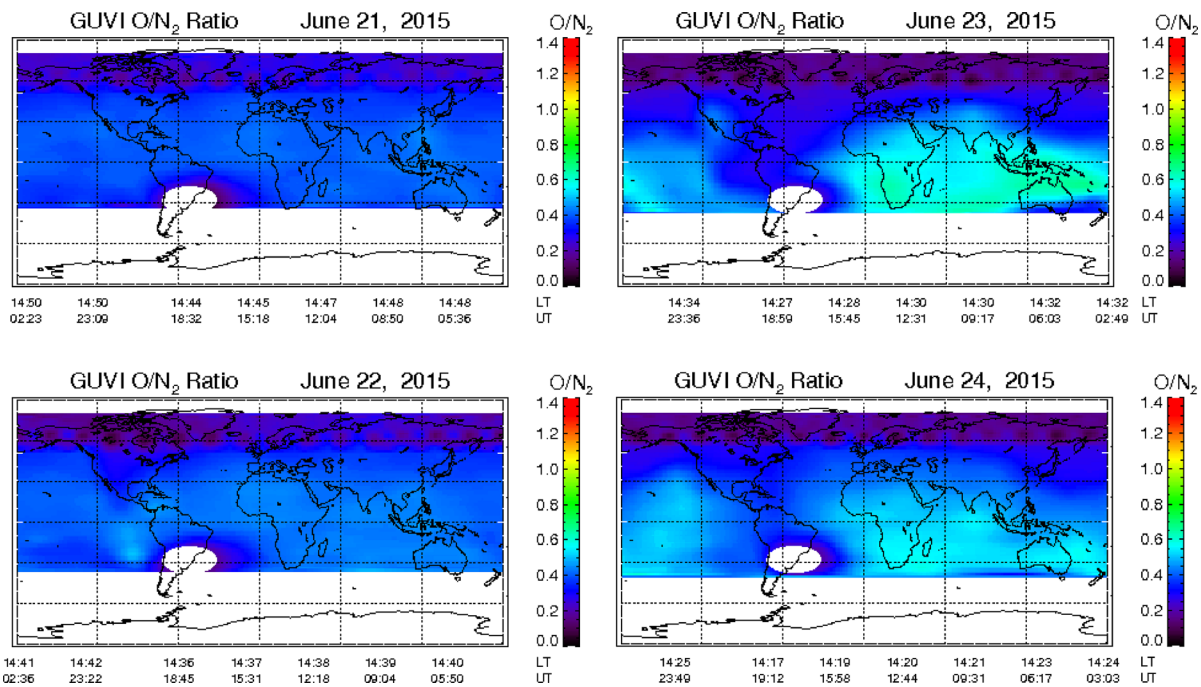

Figure 9
Global map of the O/N_2 ratio obtained by GUVI on 21–24 June (days 23 and 24, part of the main phase and recovery)

O/N_2 ratio is not surprising because the foF2 parameter (or the peak electron density NmF2) based on which the ionospheric storm effects are characterized, has a behavior which is often is different from the TEC response. For example, we can have positive effects (increases in the peak electron density) due to a simple uplifting of the F2 layer, which many have as consequence a redistribution of the ionization, but the overall effect in TEC can be zero.

4.2. *Positive Disturbances*

The increases in the electron density at middle latitudes can be provoked by the storm-time-enhanced neutral wind, which lifts up the ionospheric F2-layer plasma along the inclined field lines or by downwelling of the gas due to storm-time-induced thermospheric circulation, i.e., increase in the O/N_2 ratio (e.g., Prölss 1995; Danilov 2001, 2013). The results obtained by GUVI indicate that positive disturbances in TEC at middle latitudes in the SH may also be explained in terms of increases in the O/N_2 ratio. Unfortunately, no O/N_2 data are available at the high latitudes of the SH but it is likely that composition changes generated in the polar region sustained the long duration positive disturbances initiated prior to the storm commencement at high latitudes. These composition changes extend to midlatitudes in different longitudinal sectors, according to observations by Astafyeva et al. (2016).

The commonly observed feature in response to geomagnetic storms is a negative storm effect without obvious shift in LT (e.g., Prölss et al. 1991; Yeh et al. 1994; Szuszczewicz et al. 1998; Kane 2005; Patowary et al. 2013; Blagoveshchensky and Sergeeva 2016). We observe a clear seasonal difference in TEC: the summer hemisphere stations presented negative disturbances during the main and recovery phases while the higher latitude stations of the winter hemisphere presented positive disturbances from before the storm commencement to the EMP, which changed to negatives during the recovery phase.

Early works have reported cases in which the electron density is greatly enhanced prior to the onset of geomagnetic storms. An important feature of pre-storm enhancements observed is that they occur both day and night. For example, Kane (1973) observed strong positive effects in the critical frequency of the F2-layer foF2 before the storm sudden commencements. Kane (2005) and Blagoveschensky et al. (2006) also observed prestorm enhancements during the storm on 28 October 2003. Buresova and Lastovicka (2007) analyzed the occurrence of the pre-storm enhancements in NmF2 (proportional to $foF2^2$) at middle latitudes over Europe and found that about 20–25% of strong storms are accompanied by sufficiently strong pre-storm enhancements. Danilov (2001) listed the pre-storm enhancements as one of the open problems of F2 region physics and suggested that perhaps soft particle precipitation in dayside cusp or magnetospheric electric field penetration might play a role in this phenomenon.

Figure 2 showed an enhancement of the AE index before storm occurs, which looks like a possible cause of a pre-storm enhancement both for peak electron density and also for TEC. Because the auroral region activity is expressed via the AE index, the enhancement of AE can be associated with the positive deviations of TEC seen at high latitudes several hours before the onset of the geomagnetic storm. It is obvious that is important to continue with the study on the pre-storm ionospheric enhancements as was already suggested because possibly have potential applications in the predictions of ionospheric weather and also will help to improve our understanding of the ionosphere, especially for the physical processes of the ionospheric storms.

At middle and low latitudes and equatorial region, the initial ionospheric response to the storms can be generally explained by disturbed electric fields, which comprise prompt penetration electric fields (PPEFs) and disturbance dynamo electric fields (DDEFs). The PPEF occurs during the IMF Bz negative interval, and about 5–12% of the associated eastward interplanetary electric field (IEF) can penetrate into the ionosphere (Astafyeva et al. 2016). In general, the PPEFs from high to low latitudes take place with sudden southward turning of IMF and rapid changes in the magnetospheric convection. This occurs during the onset or main phase of the storm. The PPEF is eastward during the daytime and westward during the nighttime (Sunda et al. 2013).

The longer-lived DDEFs occur in the ionosphere during geomagnetically disturbed periods, which are driven by the storm-time neutral winds through action of the ionospheric dynamo processes (e.g., Blanc and Richmond 1980). It has opposite polarity to that of the PPEF i.e. westward during daytime and eastward during nighttime (Blanc and Richmond 1980; Fejer 1997). Their effect on the ionosphere may be felt over periods of several hours to days after geomagnetic storms.

Figure 10 shows the interplanetary electric field provided by OMNIweb data (NASA, Goddard Space Flight Center, http://omniweb.gsfc.nasa.gov) for the period 21–24 June 2015. This electric field was computed as $\mathbf{E} = -\mathbf{V} \times \mathbf{Bz}$. It can be seen a significant peak of about 18 mV/m at 16–18 UT on 22 June followed by a decrease and then by an oscillating behavior during 23 June, which presented two peaks (16 and 9 mV/m). The huge and simultaneous positive disturbances observed at low and middle latitudes, which begin to occur within an hour or so of the onset of the main phase (e.g., Darwin, Cocos Is., Townsville, Perth, Canberra, Norfolk and Brisbane) could be associated with the sharp enhancement of the electric field, because to produce these effects is required a fairly rapid mechanism. It is unlikely that the initial positive disturbances were produced by equatorward-directed meridional winds carried along by travelling atmospheric disturbances (Prölss, 1993) because several hours are required for the generation and propagation from high to low latitudes of these storm winds.

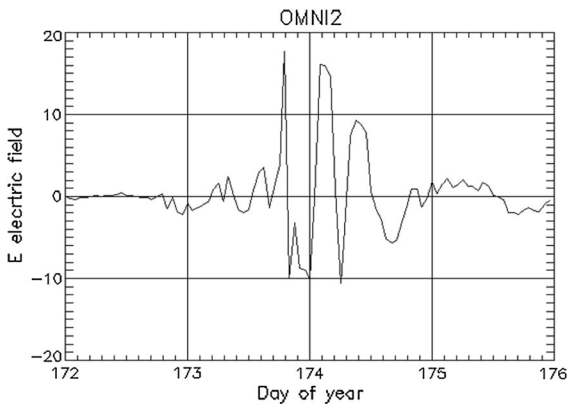

Figure 10
Interplanetary electric field ($-\mathbf{V} \times \mathbf{Bz}$) during 21–24 June 2015

The positive disturbances occurred in longitudes where the PPEF acted in the morning—noon local time sector. This result agrees with positive ionospheric storm effects observed at low and midlatitudes during a super plasma fountain (e.g., Kelley et al. 2004; Balan et al. 2009). The initial negative disturbances over equatorial latitudes also could be explained in terms of a PPEF. Because the PPEF is eastward during the daytime, it enhances the daytime eastward zonal electric field and uplifts the equatorial ionospheric plasma to higher altitudes modifying the profile of the electron density (and therefore TEC) of this region. However, this mechanism does not explain the negative disturbances initiated a few hours after local noon (during the main phase) at low latitudes of the NH.

5. *Conclusions*

This paper investigates the global variation of the Total Electron Content (TEC) in response to the geomagnetic storm of 22 June 2015 (one of the strongest geomagnetic storms of the current Solar Cycle 24). Remarkable decreases in TEC at mid-latitude stations throughout the Northern Hemisphere (summer) were observed during the development of the main phase. Prompt penetration electric fields play an important role for the increases in TEC observed at equatorial and low latitudes at the beginning of the geomagnetic storm. Increases in TEC were observed in the Southern Hemisphere (winter), which correlated well with increases in the O/N_2 ratio. However, further studies are needed to determine other possible causes for the negative disturbances that have no associated decreases in the O/N_2 ratio.

References

Abdu, M. A. (1997). Major phenomena of the equatorial ionosphere-thermo- sphere system under disturbed conditions. *Journal of Atmospheric and Solar-Terrestrial Physics, 59*(13), 1505–1519.

Astafyeva, E., Zakharenkova, I., & Alken, P. (2016). Prompt penetration electric fields and the extreme topside ionospheric

response to the June 22–23, 2015 geomagnetic storm as seen by the Swarm constellation. *Earth, Planets and Space, 68,* 152.

Astafyeva, E., Zakharenkova, I., & Förster, M. (2015). Ionospheric response to the 2015 St. Patrick's Day storm: A global multi-instrumental overview. *Journal of Geophysical Research Space Physics, 120,* 9023–9037. https://doi.org/10.1002/2015JA021629.

Balan, N., Shiokawa, K., Otsuka, Y., Watanabe, S., & Bailey, G. (2009). Super plasma fountain ionization anomaly during penetration electric fields. *Journal of Geophysical Research, 114,* A03310. https://doi.org/10.1029/2008JA013768.

Blagoveschensky, D. V., MacDougall, J. W., & Piatkova, A. V. (2006). Ionospheric effects preceding the October 2003 Halloween storm. *Journal of Atmospheric and Solar-Terrestrial Physics, 68,* 821–831.

Blagoveshchensky, D. V., & Sergeeva, M. A. (2016). Ionosphere dynamics in the auroral zone during the magnetic storm of March 17–18, 2015. *Journal of Atmospheric and Solar-Terrestrial Physics*. https://doi.org/10.1016/j.jastp.2016.06.016.

Blanc, M., & Richmond, A. D. (1980). The ionospheric disturbance dynamo. *Journal of Geophysical Research, 85,* 1669–1686.

Bounsanto, M. J. (1999). Ionospheric storms—A review. *Space Science Reviews, 88,* 563–601.

Buresova, D., & Lastovicka, J. (2007). Pre-storm enhancements of foF2 above Europe. *Advances in Space Research, 39,* 1298–1303.

Danilov, A. D. (2001). F2-region response to geomagnetic disturbances. *Journal of Atmospheric and Solar-Terrestrial Physics, 63,* 441–449.

Danilov, A. D. (2013). Ionospheric F-region response to geomagnetic disturbances. *Advances in Space Research, 52,* 343–366.

Danilov, A. D., & Lastovicka, J. (2001). Effects of geomagnetic storms on the ionosphere and atmosphere. *International Journal of Geomagnetism and Aeronomy, 2*(3), 209–224.

Fejer, B. G. (1997). The electrodynamics of the low latitude ionosphere: recent results and future challenges. *Journal of Atmospheric and Solar-Terrestrial Physics, 59,* 1456–1482.

Fuller-Rowell, T. J., Codrescu, M. V., Moffett, R. J., & Quegan, S. (1994). Response of the thermosphere and ionosphere to geomagnetic storms. *Journal of Geophysical Research, 99,* 3893–3914.

Gonzales, W. D., Joselyn, J. A., Kamide, Y., Kroehl, H. W., Rostoker, G., Tsurutani, B. T., et al. (1994). What is geomagnetic storm? *Journal of Geophysical Research, 99,* 5771–5792.

Habarulema, J. B., McKinnell, L.-A., Burešová, D., Zhang, Y., Seemala, G., Ngwira, C., et al. (2013). Comparative study of TEC response for the African equatorial and mid-latitudes during storm conditions. *Journal of Atmospheric and Solar-Terrestrial Physics, 102,* 105–114.

Kane, R. P. (1973). Global evolution of F2-region storms. *Journal of Atmospheric and Solar-Terrestrial Physics, 35,* 1953–1966.

Kane, R. P. (2005). Ionospheric foF2 anomalies during some intense geomagnetic storms. *Annales Geophysicae, 23,* 2487–2499.

Kelley, M. C., Vlasov, M. N., Foster, J. C., & Coster, A. J. (2004). A quantitative explanation for the phenomenon known as storm-enhanced density. *Geophysical Research Letters, 31,* L19809. https://doi.org/10.1029/2004GL020875.

Mendillo, M. (2006). Storms in the ionosphere: Patterns and processes for total electron content. *Reviews of Geophysics, 44*(RG4001), Paper number 2005RG000193.

Patowary, R., Singh, S. B., & Bhuyan, K. (2013). Latitudinal variation of F2-region response to geomagnetic disturbance. *Advances in Space Research, 52,* 367–374.

Prölss, G. W. (1993). Common origin of positive ionospheric storms at middle latitudes and the geomagnetic activity effect at low latitudes. *Journal of Geophysical Research, 98,* 5981–5991.

Prölss, G. W. (1995). Ionospheric F region storms. In H. Volland (Ed.), *Handbook of atmospheric electrodynamics*. Boca Raton: CRC Press.

Prölss, G. W., Brace, L. H., Mayr, H. G., Carignan, G. R., Killeen, T. L., & Klobuchar, J. A. (1991). Ionospheric storm effects at subauroral latitudes: A case study. *Journal of Geophysical Research, 96*(A2), 1275–1288.

Rishbeth, H. (1991). F-region storms and thermospheric dynamics. *Journal of Geomagnetism and Geoelectricity, 43,* 513–524.

Rishbeth, H., & Garriott, O. K. (1969). *Introduction to ionospheric physics. International geophysics series* (Vol. 14). London: Academic Press.

Singh, R., & Sripathi, S. (2017). Ionospheric response to 22–23 June 2015 storm as investigated using ground based ionosondes and GPS receivers over India. *Journal of Geophysical Research Space Physics*. https://doi.org/10.1002/2017JA024460. **(in press)**.

Sunda, S., Vyas, B. M., & Khekale, P. V. (2013). Storm time spatial variations in TEC during moderate geomagnetic storms in extremely low solar activity conditions (2007–2009) over Indian region. *Advances in Space Research, 52,* 158–176.

Szuszczewicz, E. P., Lester, M., Wilkinson, P., Blanchard, P., Abdu, M., Hanbaba, R., et al. (1998). A comparative study of global ionospheric responses to intense magnetic storm conditions. *Journal of Geophysical Research, 103*(A6), 11665–11684.

Yeh, K. C., Ma, S. Y., Lin, K. H., & Conkrigh, R. O. (1994). Global ionospheric effects of the October 1989 geomagnetic storm. *Journal of Geophysical Research, 99*(A4), 6201–6218.

(Received August 15, 2017, revised November 24, 2017, accepted November 27, 2017, Published online November 29, 2017)